Journal of Radiation Research and Applied Sciences

ISSN: (Print) (Online) Journal homepage: https://www.tandfonline.com/loi/trra20

Development of an electrostatic precipitator prototype to reduce exposure to radon progeny in poorly ventilated workplaces

V. Colenghi , L. Lepore , C. Di Carlo , F. Bochicchio & R. Remetti

To cite this article: V. Colenghi , L. Lepore , C. Di Carlo , F. Bochicchio & R. Remetti (2020): Development of an electrostatic precipitator prototype to reduce exposure to radon progeny in poorly ventilated workplaces, Journal of Radiation Research and Applied Sciences

To link to this article: https://doi.org/10.1080/16878507.2020.1838039

Published online: 05 Nov 2020.

JOURNAL OF RADIATION RESEARCH AND APPLIED SCIENCES
https://doi.org/10.1080/16878507.2020.1838039

Development of an electrostatic precipitator prototype to reduce exposure to radon progeny in poorly ventilated workplaces

V. Colenghi[a], L. Lepore[b], C. Di Carlo[a,c], F. Bochicchio[c] and R. Remetti[a]

[a]Department of Basic and Applied Sciences for Engineering, Sapienza – University of Rome, Rome, Italy; [b]Nuclear Material Characterization Laboratory and Nuclear Waste Management, ENEA Casaccia Research Center, Rome, Italy; [c]National Center for Radiation Protection and Computational Physics, Italian National Institute of Health, Rome, Italy

ABSTRACT

Electrostatic precipitation is a well-known technology to reduce public exposure to radon daughters. A custom electrostatic precipitator (ESP) prototype has been designed and built to study the effectiveness of such a removal technique in specific workplaces having low-to-zero air exchange rates with external environments. An appropriate mathematical model has been set up in order to simulate the behavior of environmental and nuclear data throughout the ESP operation, to optimize the design for the prototype to be built, to estimate its effectiveness in terms of effective dose reduction. Reference detectors have been used to measure both the radon concentration and the potential alpha energy concentration of its decay products. After a full calibration procedure, two main experiments have been performed in a room satisfying the requirements of very low ventilation rate and high radon concentration. The effective dose rate after an ESP continuous working period of either 3 h or 5 h turned out to be 50% lower than the value measured before ESP switching ON. The main contribution to dose reduction was found to be given by the first 2 hours of operation.

ARTICLE HISTORY
Received 17 May 2020
Accepted 11 October 2020

KEYWORDS
Radon; radon daughters; electrostatic precipitator; ESP; effective dose reduction

1. Introduction

Internal exposure due to inhalation of short-lived alpha emitters (or radon decay products, RDPs), i.e., ^{218}Po, ^{214}Pb, ^{214}Bi and ^{214}Po, represents a well-known public health issue (United Nations Scientific Committee on the Effects of Atomic Radiation, 2008). In the indoor ambient air, short-lived daughters tend to attach to the environmental dust following complex patterns that have been theorized and experimentally verified by some authors in the past (Porstendörfer, 1994; Porstendörfer et al., 1987, 1978). The inhaled short-lived daughters undergo radioactive decay, emitting ionizing particles which can lose energy by ionization inside the lung tissues, leading to DNA damages (World Health Organization, 2010). Three factors mainly affect the indoor concentration of radon and its RDPs: the source terms (i.e. soil, building materials, water, and outdoor air), the air exchange rate with external environments (or ventilation rate) and all the physical and chemical processes through which radon and its RDPs are 'transformed' and removed (Nazaroff & Nero, 1988). In already existing buildings, other than interventions aimed at reducing the source terms (mainly the radon entry from the soil), common remedial approaches include an increase of the ventilation rate or the use of air treatment systems, which directly reduce RDPs' concentration (United Nations Scientific Committee on the Effects of Atomic Radiation, 2000).

Electrostatic precipitators (in the following referred to as 'ESPs') belong to the latter technique, and their effect on exposure to radon daughters has been studied since the late '80s (Jonassen & Jensen, 1988; Maher et al., 1987; Moeller et al., 1986; Rajala et al., 2004; Rudnick et al., 1983; Yuan et al., 2016).

This paper investigates the effectiveness of a newly designed custom ESP electrostatic precipitator to be used in specific workplaces having typically low-to-zero air exchange rates with external environments. An appropriate mathematical model, based on Jacobi-Porstendörfer's room model (Porstendörfer et al., 2005), has been developed in order to evaluate the effectiveness of the custom-designed electrostatic filter. The ESP has undergone commissioning and calibration tests in poorly ventilated rooms that represent the target scenario for the device application.

2. Materials and methods

2.1. Modeling radon decay products precipitation

A room model code, based on the Jacobi-Porstendörfer's (Porstendörfer et al., 2005), has been created to simulate the ESP performance as a function of its layout. The actual effectiveness of the device has been so quoted in terms of effective dose reduction. The processes affecting concentrations and granulometric distributions of attached and unattached

CONTACT C. Di Carlo christian.dicarlo@iss.it

fractions of ^{218}Po, ^{214}Pb, ^{214}Bi, and ^{214}Po have been simulated taking into account diffusivity, attachment to, and desorption from, aerosol particles and deposition rates on solid surfaces of each decay product. An algorithm has been developed to compute the distribution of activity among attached and unattached radon daughters in a given room over time. The radon concentration has been treated as an input quantity. The model is based on an 8-equations system, two for each of the four short-lived decay products, adapted from Jacobi- Porstendörfer's. Considering the very short half-life of ^{214}Po, compared to ^{214}Bi's, the equations reduce to six by the assumption of secular equilibrium between the latter two nuclides. For each of the remaining three short-lived decay products, the following two equations have been considered:

$$C^f_{j,i} = C^f_{j,(i-1)} + \Delta t \cdot \left[\lambda_j \cdot C^f_{(j-1),i} + R_{(j-1)} \cdot \lambda_j \cdot C^a_{(j-1),i} - S^f_{j,i} \cdot C^f_{j,(i-1)}\right] \quad (1)$$

$$C^a_{j,i} = C^a_{j,(i-1)} + \Delta t \cdot \left[\left(1 - R_{(j-1)}\right) \cdot \lambda_j \cdot C^a_{(j-1),i} + X_{r,i} \cdot C^f_{j,i} - S^a_{j,i} \cdot C^a_{j,(i-1)}\right] \quad (2)$$

where:

- the apexes *f* and *a* indicate the unattached (or free) and attached fraction of the radon daughters, respectively;
- the subscript *j* varies in the range 1–3, and it refers, in order, to ^{218}Po, ^{214}Pb, and ^{214}Bi. When *j*=0, the corresponding quantity is referred to ^{222}Rn;
- the subscript *i*indicates the time step, beginning from $i = 1$;
- C_j stands for the (attached or free) activity concentration of nuclide *j*, in [Bq m^{-3}];
- $\Delta t = t_i - t_{(i-1)}$ is the magnitude of the time step, in [s];
- λ_j is the decay constant of nuclide *j*, in [s^{-1}];
- R_j is the recoil probability of the radioactive decay considered ($R_0 = 0$, $R_1 = 0.8$, $R_2 = 0$);
- X_r is the attachment rate, in [s^{-1}];
- S_j is the total removal parameter for nuclide *j*, differently defined for the attached and unattached fraction, in [s^{-1}].

2.1.1. Attachment rate X_r

The attachment rate, which is a function of time, has been evaluated through the linear relationship proposed by (Porstendörfer, 1994; Stevanovic et al., 2010):

$$X_{r,i} = \bar{\beta}\, Z_{p,\,i} \quad (3)$$

where:

- β is the attachment coefficient. In calculations, a value averaged over the entire particles diameter range, $\bar{\beta} = 2 \cdot 10^{-6}$ cm^3 s^{-1} (slightly greater than that proposed in 2001 (Porstendörfer, 2001)), has been considered for the attachment coefficient.
- $Z_p(t)$ is the total particle number concentration, standing for the integral of the dust concentration over the entire dust diameter distribution, $Z_p(t) = {}^{Z_p}(d_p, t)\mathrm{d}(d_p)$.

2.1.2. Removal parameter, S_j

For each radionuclide, the removal parameter S_j has been separately evaluated in [s^{-1}] for the free and the attached fraction (Porstendörfer et al., 2005):

$$S^f_{j,i} = v_r + \lambda_j + q^f + X_{r,i} + \frac{\Gamma_{\mathrm{ESP}} \cdot \eta^f}{V_r} \quad (4)$$

$$S^a_{j,i} = v_r + \lambda_j + q^a + \frac{\Gamma_{\mathrm{ESP}} \cdot \eta^a}{V_r} \quad (5)$$

where in turn:

- v_r is the ventilation rate in the room, in [s^{-1}];
- q^f and q^a are the unattached and attached fraction deposition rate, in [s^{-1}], respectively. They have been computed by means of a linear relationship with respect to the ratio between the room's surface and volume (Porstendörfer et al., 1978);
- Γ_{ESP} is the volumetric air flow through the ESP, in [m^3 s^{-1}];
- V_r is the room volume, in [m^3];
- η_f and η_a are the ESP collection efficiencies for the free and the attached fraction, respectively.

The model is discretized in time in order to easily approach the several time-dependent variables. The resulting finite difference model works under the following simplifying assumptions:

- perfect and instantaneous mixing between radon, its daughters and other air components, so that the averaged activity concentration can be assumed to be the actual one in every cubic meter of air;
- radon activity concentration is given as an input every 10 min, thus no models for radon exhalation were used. In every ten-minutes interval, the concentration is so assumed to vary linearly between the values registered at the beginning and at the end of that period;
- a total particle number concentration, standing for the integral of dust diameter distribution, has been considered, $Z_p = 5000$ cm^{-3};
- the removal parameters for radon daughters are ventilation, attachment to ambient aerosol (if

unattached), deposition on wall surfaces, radioactive decay and the ESP, if switched ON;
- constant recoil probabilities: 80% for the $^{218}Po \rightarrow {}^{214}Pb$ decay, and 0% for the $^{218}Pb \rightarrow {}^{214}pb$;
- activity concentration distribution vs. diameter for unattached and attached fractions has been modeled according to Table 1:
- particle charge is not considered;
- when the ESP was turned OFF, deposition velocities of attached, u^a, and unattached fractions, u^f, have been set to $3 \cdot 10^{-3}$ cm s^{-1} and 0.8 cm s^{-1} (Porstendörfer et al., 1978), respectively. When the ESP was turned ON, due to the increase in air flow velocity nearby the precipitator, both deposition velocities have been gradually increased up to double their original values;
- thoron and its daughters are not included in the model because their contribution to the annual effective dose is much lower than that from radon and RDPs (United Nations Scientific Committee on the Effects of Atomic Radiation, 2000);
- during the ESP functioning (i.e. power ON), no aerosol sources have been considered by the room model;
- ESP fouling is not considered, so ESP efficiencies are considered as time-independent quantities.

2.1.3. ESP collection efficiency

The collection efficiency of the electrostatic precipitator has been computed by considering the sum of the efficiencies, function of the AMDs in Table 1, weighted by the corresponding probability, p_i^k. The formulation is the same for the attached ($k = a$) and the unattached ($k = f$) fraction.

$$\eta^k = \sum_{i=1}^{3} p_i^k \, \eta\left(\mathrm{AMD}_i^k\right) \tag{6}$$

The AMD-dependent collection efficiency, $\eta\left(\mathrm{AMD}_i^k\right)$, has been evaluated through the Deutsch-Anderson equation (Deutsch, 1925; Robinson, 1919) appropriately modified for multi-duct configuration:

Table 1. Summary of assumed values for activity concentration distribution as a function of particle diameter for unattached and attached fractions. Activity overall distributions for unattached and attached fraction are both assumed as the sum of three distributions each characterized by specific probability and activity median diameter (AMD).

Unattached activity distribution		Attached activity distribution	
p^f [%]	AMD^f [nm]	p^a [%]	AMD^a [nm]
13	0.60	70	280
35	0.85	25	30
52	1.25	5	4000

$$\eta\left(AMD_i^k\right) = 1 - e^{-\frac{S_{col}}{\Gamma_{ESP}} u_d} \tag{7}$$

where Γ_{ESP} [m^3 s^{-1}] is the volumetric air flow through the ESP section, S_{col} [m^2] is the sum of all the ESP's collection surfaces, and u_d is the drift velocity [m s^{-1}], whose expression was recovered from the force balance (Arendt & Kallmann., 1926; Benitez, 1993; Falaguasta et al., 2008; Friedlander, 2000; Hinds, 1999; National Research Council, 1991; Pauthenier & Moreau-Hanot, 1932; Ruttanachot et al., 2011; White, 1962).

2.2. Design and set-up of the electrostatic precipitator

The mathematical model discussed before has led to the identification of an optimal design for the prototype to be realized and tested. Figure 1 shows both the AutoCAD 3D layout and the realized device. It is conceived as a parallelepiped, 7-duct, wire-plate, dry ESP with positive DC power supply. The metallic plates are thin 1000 × 350 mm aluminum foils. They exhibit certain flexibility, and this could represent an issue for their use under high air flows. For this reason, the air flow could not be too high, both to let the aluminum plates stay in place and to avoid an excessive particle re-entrainment (Chang et al., 2018; Mizuno, 2000; White, 1974). 5 cm has been chosen as plate-to-plate distance being the latter the minimum distance that allows the builders to substitute eventually damaged wires without having to disassemble the whole prototype. The chosen distance has been observed to be narrow enough to lower the corona inception electric field value, hence the operational voltage.

The HV-in pins are placed on the top of the prototype, while the ground pin is on one of the sides. All the collecting electrodes (the aluminum plates) are electrically connected to the ground pin. The emitting electrodes, copper wires with a diameter of 0.25 mm, were arranged in a 5 × 7 matrix, all electrically connected to the HV-in pins. The wires characteristics, number, and collocation were chosen as a compromise between mechanical resistance, inexpensiveness, and functionality (Boelter & Davidson, 1997; Mizuno, 2000; Peek, 1915).

The maximum voltage to be applied to the ESP prototype was set around 10 kV. A positive direct current (DC) ESP supply was chosen to enhance particle collection (White, 1962) and reduce ozone generation rate (Yehia et al., 2000). The power supply design that better fitted all the constraints was a modified and more stabilized version of an original drawing ('The Basic Transdimensional's Lifter Experiment by JL Naudin,' n.d.) based in turn on a Royer oscillator (Royer, 1954). The primary side of the low voltage (LV) to high voltage (HV) transformer was, in turn, supplied by a stabilized voltage generator whose output ranges between 10 and 24 V (DC).

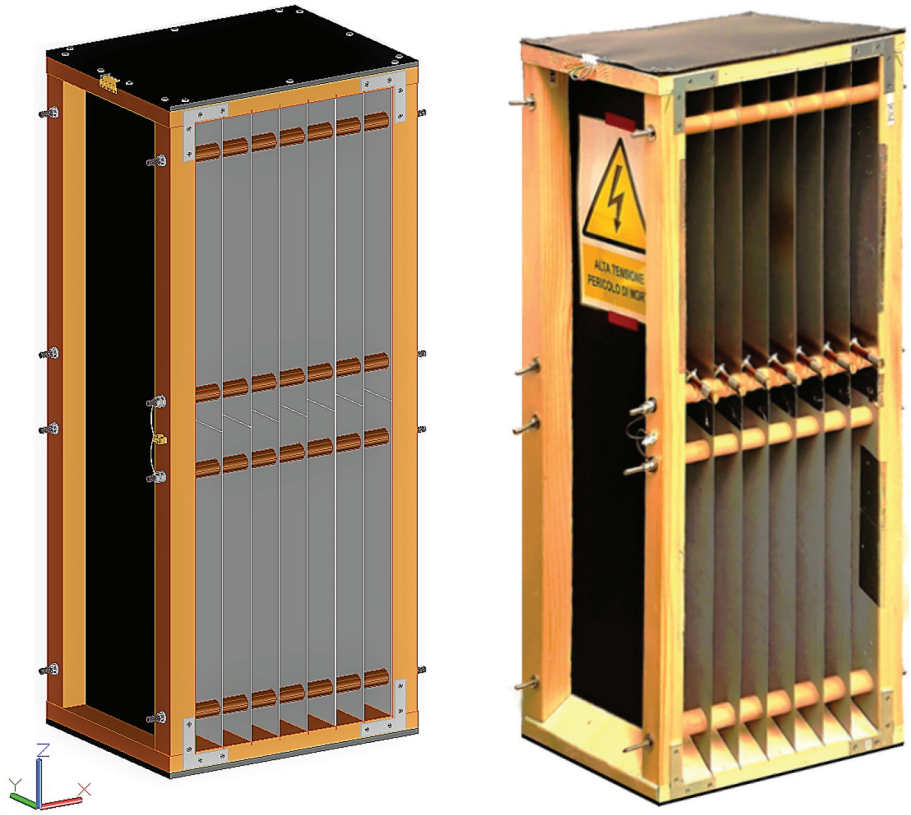

Figure 1. On the left, the completed ESP AutoCAD 3D (Autodesk software) model, on the right, the actually realized prototype.

2.2.1. Electrical characterization of the prototype

Appropriate electrical safety measures were taken before coupling the HV power supply with the ESP prototype.

The prototype has been electrically characterized by performing a series of measurements with step-by-step variations of low voltage in the primary side of the power supply. As a result of this, the operating high voltage of the ESP has been set to 8 kV. The corresponding total corona current of the emitting electrodes has been measured to be about 1 mA, showing a very good agreement with theoretical results obtained by applying previous literature relations (Cooperman, 1960; Townsend, 1915).

2.3. Reference instrumentation for detection of radon and its progeny

Potential alpha energy concentration (PAEC) of both attached and unattached fractions of radon progeny has been measured by the reference detector TracerLab BLWM-PLUS-2S (Tracerlab Gmbh, n.d.). The latter is an active radon/thoron-progeny-monitor, designed as a 2-channels monitor, each with an independent sampler: one for the determination of the overall PAEC and one for the determination of the only unattached fraction. Measurements have been carried out by using either the 'continuous slow' operating algorithm, with a small statistical uncertainty even at small concentrations and a large time constant for changes in concentrations (2 hours for 80%), and the 'continuous fast' algorithm, with a higher statistical uncertainty but a significantly lower time constant for changes. The instrument has been put on a surface nearby the ESP's air flow outlet, but on a side, to avoid both flow instabilities and malfunctioning in the instrument detection capabilities.

The continuous radon monitor AlphaGUARD PQ2000 (Genitron InstrumentGmbH, 2012) has been employed to measure indoor radon concentration as well as some environmental parameters, i.e., pressure, temperature, relative humidity. The detector is an ion chamber monitor and has the highest sensitivity among radon continuous monitors available on the market (0.05 cpm Bq^{-1} m^3) as well as a wide measuring range of 2–2,000,000 Bq m^{-3}. It has been operating in diffusion mode returning its outputs every 10 minutes.

3. Design of experiments

A tower fan, with a parallelepiped air-outlet of 60 × 600 mm, has been connected to the ESP inlet via a trapezoid diffuser, 80 cm long (Figure 2).

The room chosen for the experiments has a volume of about $V_r = 180$ m^3, and it was characterized by relatively high indoor radon-concentrations, about 800 Bq m^{-3} as a yearly averaged value. The total attachment surface (i.e. walls, furniture, and objects in the room) has been estimated to be $S_r = 160$ m^2.

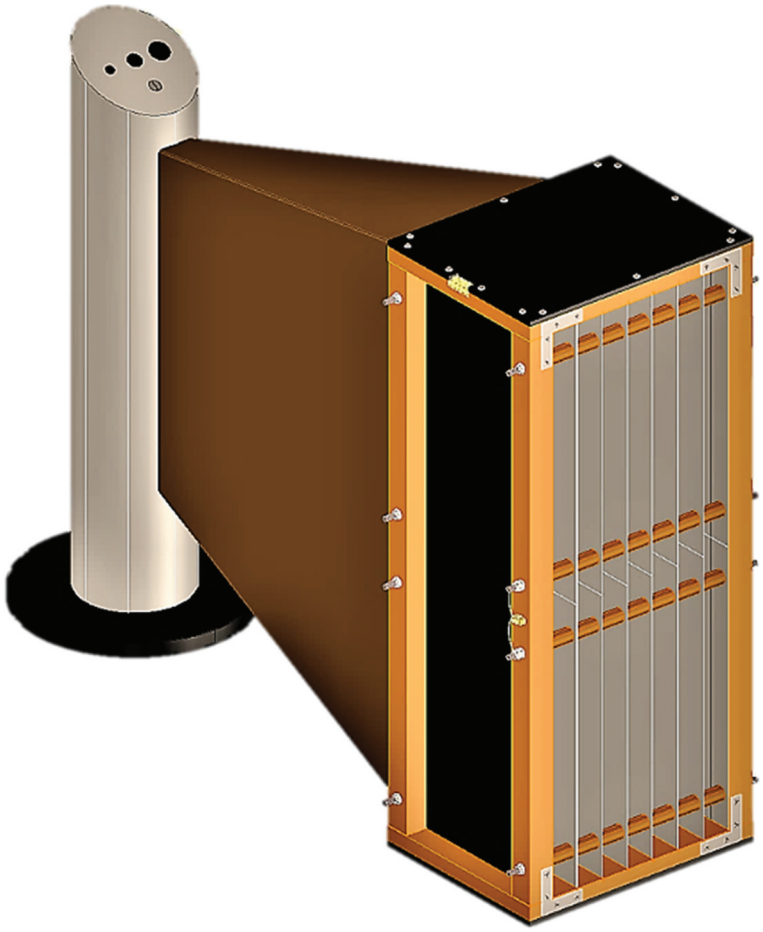

Figure 2. AutoCAD 3D model of the geometrical configuration chosen to couple the ESP with the tower fan.

When the ESP was OFF the ventilation rate, v_r, turned out to be 0.5 h^{-1}. Switching ON the fan has been found to produce an increase of about 1.3 times in v_r.

The dust particles concentration Z_p has been predicted by means of the relation $Z_p = 414/f_p$ (Porstendörfer, 2001).

The ESP prototype was put in the center of the room, away from any furniture that could interfere with the air flow.

All the instruments have been connected to a single multi-socket unit, provided with an inborn emergency stop button. The unit was then brought out from the room where a working station was organized to allow the operator to check the high voltage level and to easily switch ON/OFF the power supply. The inside of the room was monitored and recorded via webcam.

At least 1 day before the experiments, after having switched ON both the TracerLab and the AlphaGUARD, all the room entrances have been closed, and the room was left unused to have a better estimation of all the relevant parameters in the undisturbed state.

4. Results and discussion

The results of two experiments are hereby discussed. The first aimed to investigate the effectiveness, in terms of effective dose reduction, of an ESP continuous operation of 3 hours. The second focused on evaluating the effects of a longer operation period, i.e., 5 hours.

4.1. Experiment 1

During this period, the radon concentration – the unchanged ventilation conditions during the experiments providing a likely explanation for it – remains almost constant (Figure 3).

The attached PAEC (black lines in Figure 4) showed a reduction of about 90%, passing through three subsequent phases: *i*) during the first hour after ESP switching ON, the attached PAEC was reduced by 50% and the mean slope of the trend, slightly concave downward, was -3.8 MeV cm^{-3} h^{-1}, *ii*) during the second hour of ESP operation, the attached PAEC was reduced by a further 30%, and the mean slope of the trend, now slightly concave upward, was -2.1 MeV cm^{-3} h^{-1}, *iii*) during the last hour of ESP functioning, the residual reduction, of less than 10%, in attached PAEC was realized while the slope gradually goes to 0 MeV cm^{-3} h^{-1}.

The actual attached removal efficiency was found to be $\eta^a = 0.18$.

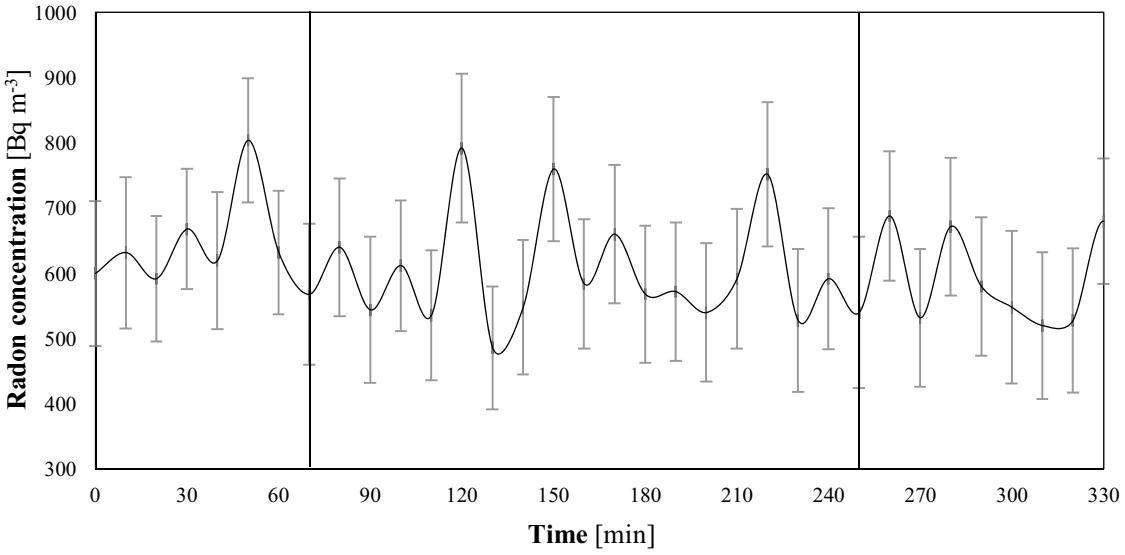

Figure 3. Radon concentration measured by AlphaGUARD PQ2000 during *Experiment 1*. The vertical lines delimit the period of ESP operation.

On the contrary, the unattached PAEC (gray lines in Figure 4) was found to be almost unchanged. This can be explained by taking into account several phenomena not considered within the theoretical model due to their actual complexity. Among them, the main role is probably of the re-entrainment (Chang et al., 2018; Mizuno, 2000; White, 1974).

During the ESP working period, both the equilibrium factor F and the unattached fraction f_p drastically vary (Figure 5): while F was observed to sharply decrease going from about 0.35 to 0.07, f_p increased from about 0.07 to 0.4. These two observed trends were clearly determined by the previously discussed behaviors of attached and unattached PAECs.

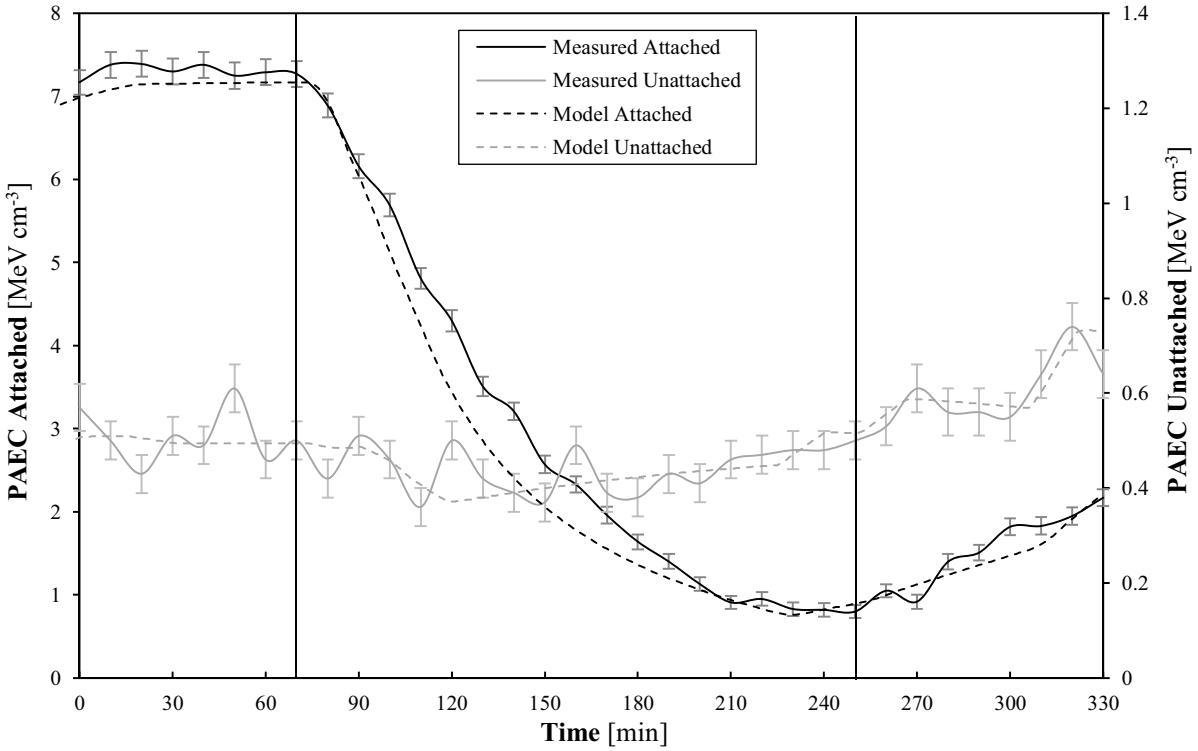

Figure 4. Measured trends for potential alpha energy concentration of attached (black) and unattached (gray) fractions during *Experiment 1*. The solid lines represent the measured values, whereas the dashed lines are the output of the model. The vertical lines delimit the period of ESP operation.

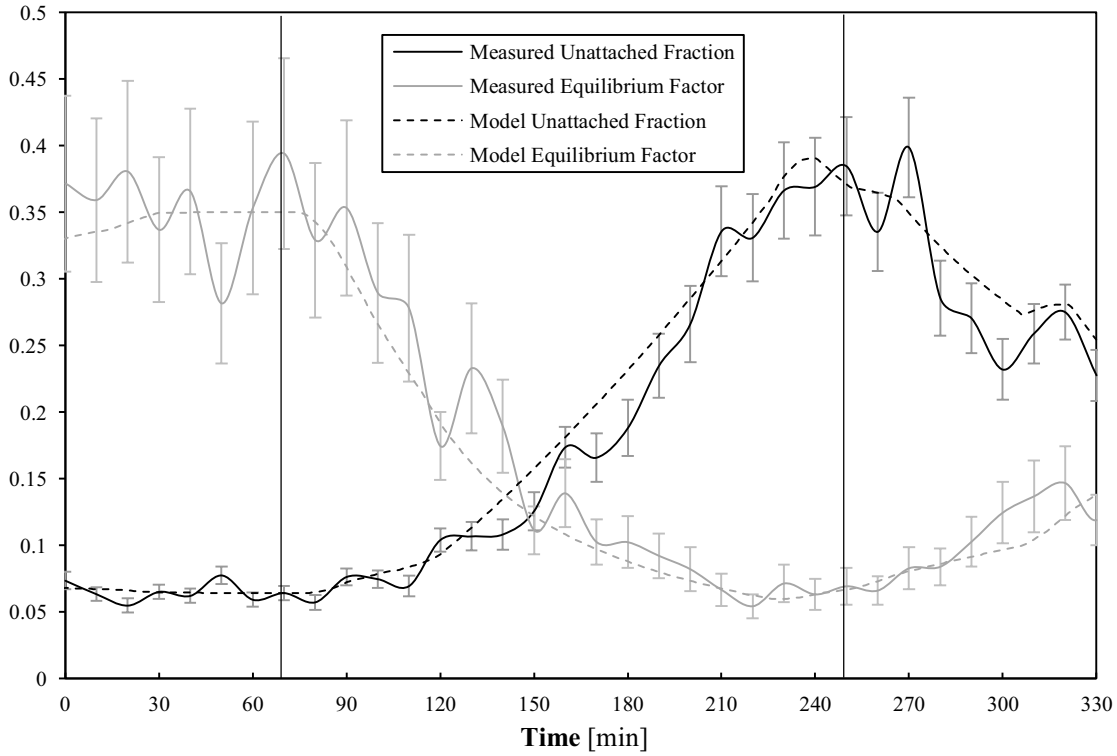

Figure 5. Measured trends for the unattached fraction f_p (black) and the equilibrium factor F (gray) during *Experiment 1*. The solid lines represent the measured values, whereas the dashed lines are the output of the model. The vertical lines delimit the period of ESP operation.

4.2. Experiment 2

During the second experiment, the radon concentration decreased from 1000 Bq m^{-3} to 750 Bq m^{-3} despite the unchanged ventilation conditions (Figure 6).

The attached PAEC (black lines in Figure 7) reduced to about 10%, passing through three subsequent phases very similar to those observed for *Experiment 1: i*) during the first 80 minutes after the ESP switching ON, the attached PAEC was reduced by 45% and the mean slope of the trend, slightly concave downward, was -4.5 MeV cm^{-3} h^{-1}, *ii*) during the following hour of ESP functioning, the attached PAEC was reduced by a further 30%, and the mean slope of the trend, now slightly concave upward, was

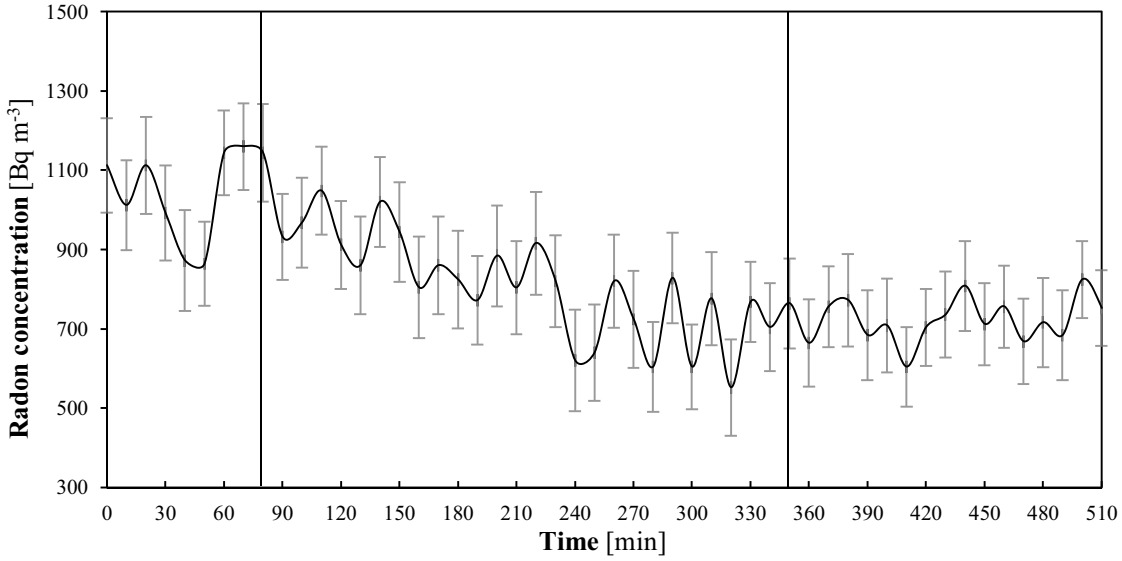

Figure 6. Radon concentration measured by AlphaGUARD PQ2000 during *Experiment 2*. The vertical lines delimit the period of ESP operation.

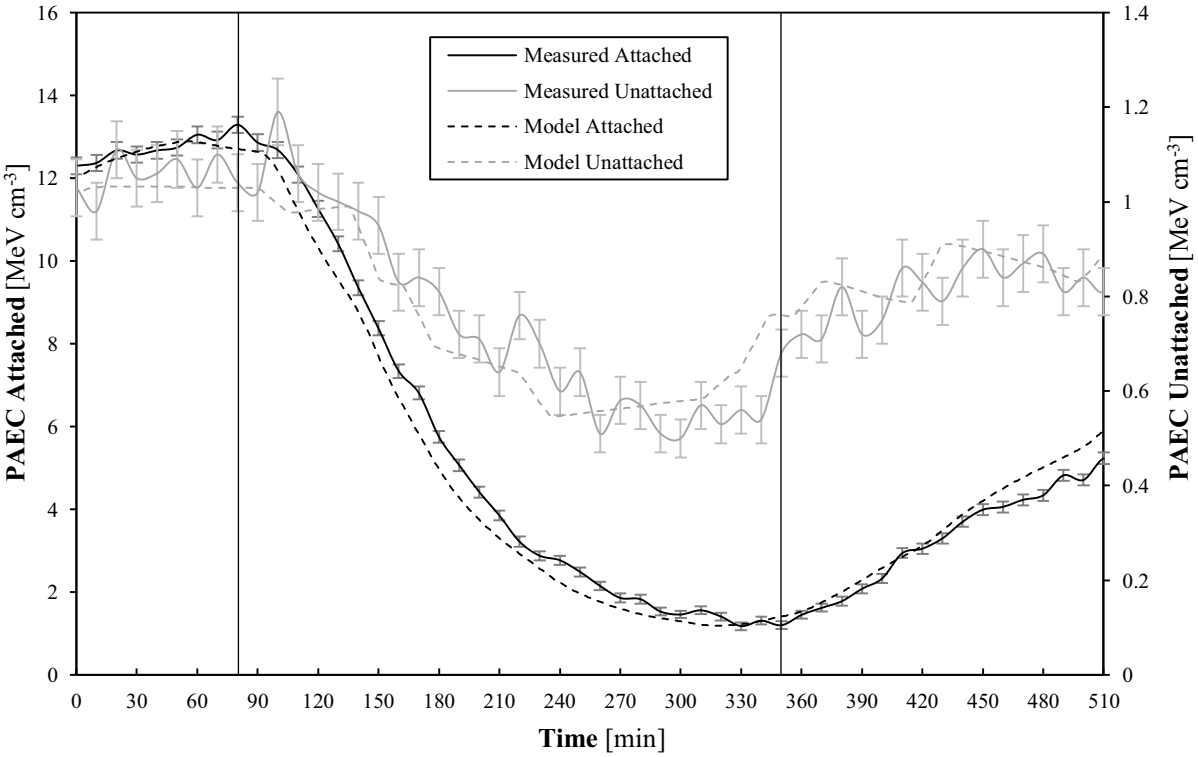

Figure 7. Measured trends for potential alpha energy concentration of attached (black) and unattached (gray) fractions during *Experiment 2*. The solid lines represent the measured values, whereas the dashed lines are the output of the model. The vertical lines delimit the period of ESP operation.

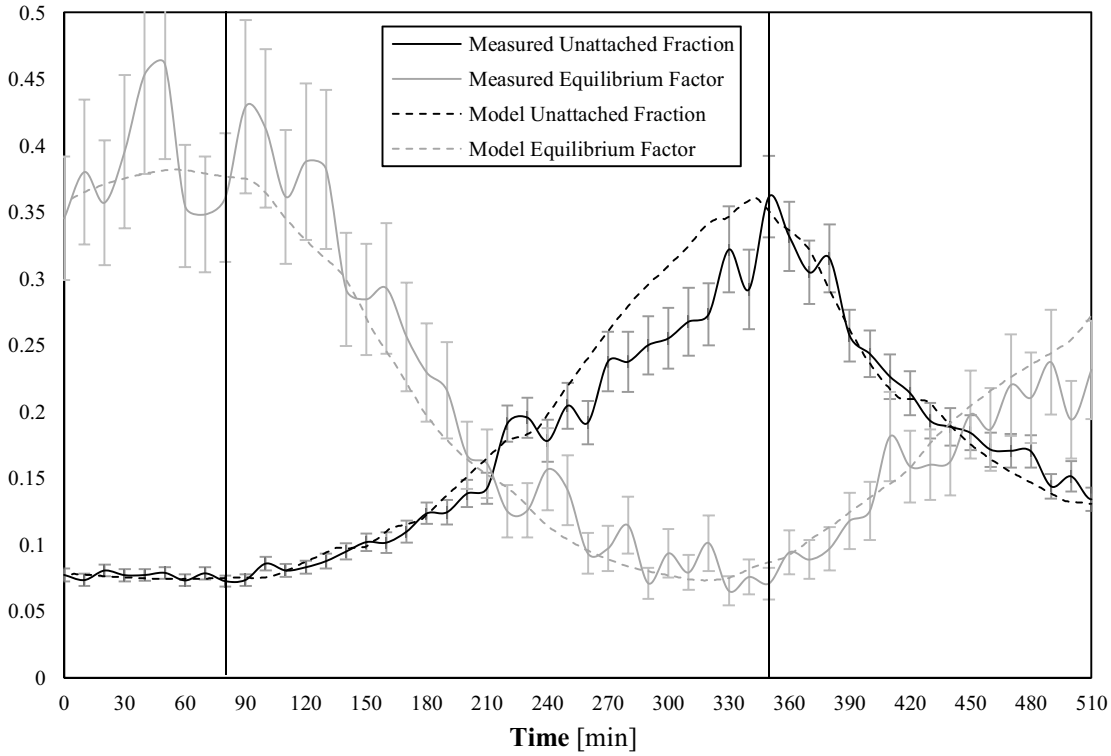

Figure 8. Measured trends for the unattached fraction f_p (black) and the equilibrium factor F (gray) during *Experiment 2*. The solid lines represent the measured values, whereas the dashed lines are the output of the model. The vertical lines delimit the period of ESP operation.

-4.1 MeV cm^{-3} h^{-1}, *iii*) during the remaining ESP working period, the further reduction, of about 15%, in attached PAEC was realized while the slope gradually went to 0 MeV cm^{-3} h^{-1}.

The actual attached removal efficiency was found to be $\eta^a = 0.12$.

As in *Experiment 1*, the unattached PAEC (gray lines in Figure 7) experienced a weak decrease (of about 20%): such trend was due to the corresponding reduction in radon concentration and it was not produced by the operation of the precipitator, for the same reasons explained before.

As shown in Figure 8, F sharply decreased from about 0.37 to 0.08, and f_p contemporarily increased from about 0.08 to 0.35.

4.3. Dose reduction efficiency

The values of the effective dose during the experiments were derived, attached and unattached values considered separately, utilizing the conversion factors (DCFs) recommended by ICRP 137 (Paquet et al., 2017) for indoor workplaces: 86 mSv WLM^{-1} (DCF^f) and 14 mSv WLM^{-1} (DCF^a) for unattached and attached fraction, respectively.

The effective dose rate trends are plotted in Figure 9 and the corresponding relative reductions listed in Table 2. For both the experiments, the strongest reduction occurred during the first hour of ESP operation: 41.5% and 26.6% for *Experiment 1* and *2*, respectively. During the second hour, the percentage reduction was about 20% in both scenarios. From the beginning of the third hour and on, the reduction in the effective dose rate due to ESP got lower and lower. During the last minutes of operation, the attached fraction was no more reduced by the ESP and the slight increase in unattached fraction reflected on an increase in the effective dose rate. Comparing effective dose rates during the first 30 minutes after the ESP switching OFF, $\dot{E}_{OFF}$, to the undisturbed values before the ESP operation, $\dot{E}_0$, shows a reduction of about 50% (55.7% and 49.8%, respectively) in both experiments.

Results suggest – for the ESP considered and the room chosen for the experiments – not to exceed 2 hours of ESP continuous operation. Indeed, even if the greatest reductions were observed during the first hour, in the following 60 minutes an appreciable contribution to dose reduction was noticed as well. Longer operation periods would not reflect in further reductions as shown by the comparison of *Experiment 1* (ESP ON for 3 h) and *Experiment 2* (ESP ON for 5 h).

5. Conclusions

A single-stage, multi-duct, dry, parallelepiped electrostatic precipitator prototype has been so designed and built to demonstrate the effectiveness of ESP technique in reducing the effective dose due to exposure to radon progeny in poorly ventilated indoor workplaces. The prototype realization has followed criteria of reliability, inexpensiveness, safety, and practicality.

The results of the tests performed in a poorly ventilated room ($v_r = 0.5$ h^{-1}) showed a net reduction of

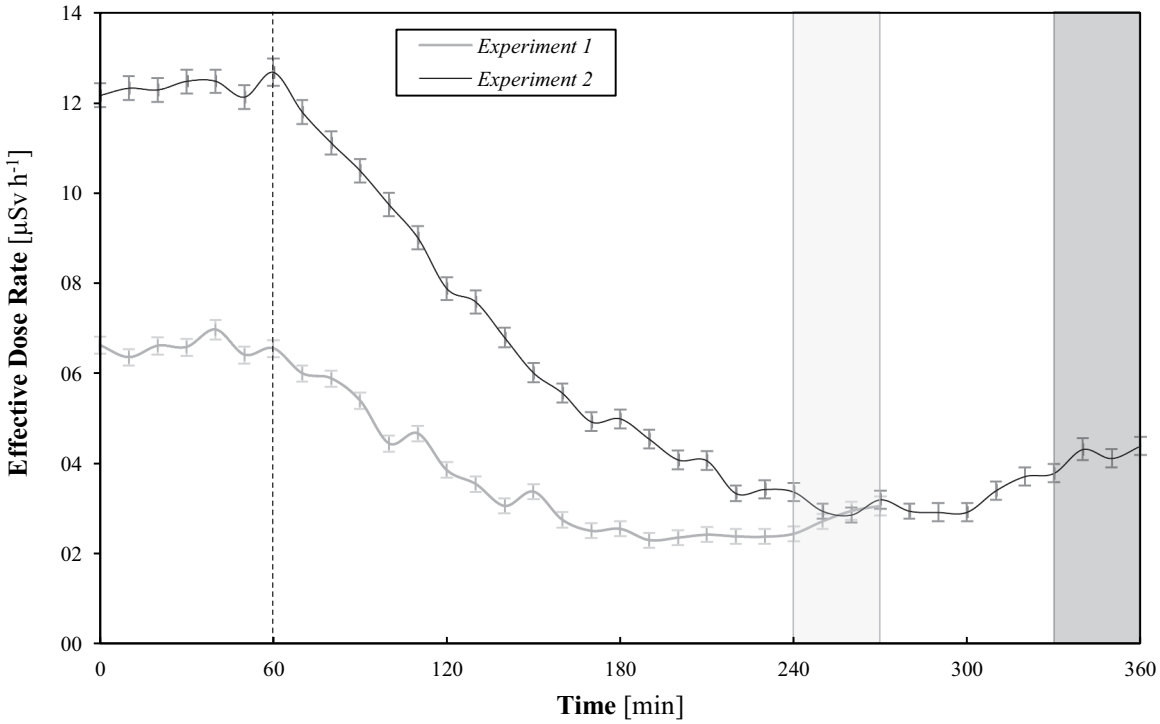

Figure 9. Measured trends of effective dose rate during *Experiment 1* and *2*. The vertical dashed line indicates the ESP switching ON. The light and dark gray boxes highlight the first 30 minutes after ESP switching OFF during *Experiment 1* and *2* respectively.

Table 2. Effective dose rate for *Experiment 1* and *2* at different times: $\dot{E}_0$ is the hourly-averaged effective dose rate immediately before the ESP operation, $\dot{E}_{1h}$ and $\dot{E}_{2h}$ are the effective dose rates measured after 1 and 2 h of ESP operation, respectively, and $\dot{E}_{OFF}$ is the 30-minutes-averaged effective dose rate after the ESP got switched OFF. Columns 3 and 5 report the relative reduction with respect to the undisturbed value $\dot{E}_0$.

Effective Dose Rate	*Experiment 1*		*Experiment 2**	
	(μSv h^{-1})	(%)	(μSv h^{-1})	(%)
$\dot{E}_0$	6.6		12.2	
$\dot{E}_{1h}$	3.9	41.5	9	26.6
$\dot{E}_{2h}$	2.6	61.2	6.3	48.8
$\dot{E}_{OFF}$	2.9	55.7	6.2	49.8

*Values for *Experiment 2*, affected by a decrease in radon concentration during ESP operation period, have been corrected to exclude the contribution of such a decrease in reducing the PAEC, and so the effective dose rate. In this way, as for *Experiment 1*, dose reductions reported for *Experiment 2* are attributable to the ESP only.

the effective dose rate: the latter, averaged over the first 30 minutes after an ESP continuous working period of either 3 h or 5 h, turned out to be 50% lower than the value measured in the last hour before switching ON the ESP. The main contribution to dose reduction was found to be given by the first 2 hours of ESP operation: 30–40% by the first hour and 20% by the second. Results seem to suggest not to operate the electrostatic precipitator for more than 2 hours, being the additional working period useless, or even harmful.

This technology, given its characteristics, could mainly be applied to remediate indoor environments that cannot be ventilated (both naturally or forcefully) and whose occupancy is always scheduled and limited to short periods (up to 1 h), e.g., bank vaults or control rooms of water treatment plants. In such scenarios, frequently interested by very high radon concentrations, the ESP could be remotely controlled and switched ON on-demand, i.e., 1–2 hours before the room needs to be entered.

Acknowledgments

The authors would like to express their gratitude to Marco Ampollini and all the Laboratory of Radioactivity of the Italian National Institute of Health for making it possible to use the TracerLab BLWM-PLUS-2S.

Disclosure statement

The authors declare that they have no known competing financial interests or personal relationships that could have appeared to influence the work reported in this paper.

ORCID

L. Lepore http://orcid.org/0000-0003-0088-6449
C. Di Carlo http://orcid.org/0000-0002-6629-7658
F. Bochicchio http://orcid.org/0000-0003-1291-3037
R. Remetti http://orcid.org/0000-0002-8786-0753

References

Arendt, P., & Kallmann., H. (1926). The mechanism of charging mist particles. *Z. Phys*, *35*, 421. https://doi.org/10.1007/BF01385419

Benitez, J. (1993). *Process engineering and design for air pollution control*. Prentice Hall.

Boelter, K. J., & Davidson, J. H. (1997). Ozone generation by indoor, electrostatic air cleaners. *Aerosol Science and Technology*, *27*(6), 689–708. https://doi.org/10.1080/02786829708965505

Chang, J.-S., Kelly, A. J., & Crowley, J. M. (2018). *Handbook of electrostatic processes*. CRC Press. https://doi.org/10.1201/9781315214559

Cooperman, P. (1960). A theory for space-charge-limited currents with application to electrical precipitation. *Transactions of the American Institute of Electrical Engineers, Part I: Communication and Electronics*, *79*(1), 47–50. https://doi.org/10.1109/tce.1960.6368541

Deutsch, W. (1925). Elektrische Gasreinigung. *Z. Tech. Phys*, *6*, 423–427.

Falaguasta, M. C. R., Steffens, J., Valdes, E. E., & Coury, J. R. (2008). Overall collection efficiency of a plate-wire electrostatic precipitator operating on the removal of PM2.5. *Latin American Applied Research, 38*, 179–186.

Friedlander, S. K. (2000). *Smoke, dust, and haze: Fundamentals of aerosol dynamics* (2nd ed.). Oxford University Press.

Genitron InstrumentGmbH. (2012). *AlphaGUARD portable radon monitor - User manual* (pp. 1–59).

Hinds, W. C. (1999). *Aerosol technology: Properties, behavior, and measurement of airborne particles* (2nd ed.). New York: Wiley.

Jonassen, N., & Jensen, B. (1988). *Removal of radon daughters by filtration and electrostatic plateout*.

Maher, E. F., Rudnick, S. N., & Moeller, D. W. (1987). Effective removal of airborne 222Rn decay products inside buildings. *Health Physics*, *53*(4), 351–356. https://doi.org/10.1097/00004032-198710000-00001

Mizuno, A. (2000). Electrostatic precipitation. *IEEE Transactions on Dielectrics and Electrical Insulation*, *7*(5), 615–624. https://doi.org/10.1109/94.879357

Moeller, D. W., Rudnick, S. N., & Maher, E. F. (1986). *Method and apparatus for reduction of radon decay product exposure*.

National Research Council. (1991). *Comparative dosimetry of radon in mines and homes*. Washington, DC: The National Academies Press. https://doi.org/10.17226/1799

Nazaroff, W. W., & Nero, A. V. (1988). *Radon and its decay products in indoor air*. John Wiley and Sons Inc.

Paquet, F., Bailey, M. R., Leggett, R. W., Lipsztein, J., Marsh, J., Fell, T. P., Smith, T., Nosske, D., Eckerman, K. F., Berkovski, V., Blanchardon, E., Gregoratto, D., & Harrison, J. D. (2017). ICRP publication 137: Occupational intakes of radionuclides: Part 3. *Annals of the ICRP*, *46*(3–4), 1–486. https://doi.org/10.1177/0146645317734963

Pauthenier, M., & Moreau-Hanot, M. (1932). La charge des particules sphériques dans un champ ionisé. *Journal De Physique Et Le Radium*, *3*(12), 590–613. https://doi.org/10.1051/jphysrad:01932003012059000

Peek, F. (1915). *Dielectric phenomena in high voltage engineering*. McGraw-Hill Book Company Inc.

Porstendörfer, J. (1994). Properties and behaviour of radon and thoron and their decay products in the air. *Journal of Aerosol Science*, *25*(2), 219–263. https://doi.org/10.1016/0021-8502(94)90077-9

Porstendörfer, J. (2001). Physical parameters and dose factors of the Radon and Thoron decay products. *Radiation Protection Dosimetry*, *94*(4), 365–373. https://doi.org/10.1093/oxfordjournals.rpd.a006512

Porstendörfer, J., Pagelkopf, P., & Gründel, M. (2005). Fraction of the positive 218Po and 214Pb clusters in indoor air. *Radiation Protection Dosimetry*, *113*(3), 342–351. https://doi.org/10.1093/rpd/nch465

Porstendörfer, J., Reineking, A., & Becker, K. (1987). F*ree fractions, attachment rates, and plate-out rates of Radon daughters in houses*. ACS Symposium Series. https://doi.org/10.1021/bk-1987-0331.ch022

Porstendörfer, J., Wicke, A., & Schraub, A. (1978). The influence of exhalation, ventilation and deposition processes upon the concentration of Radon (222Rn), Thoron (220Rn) and their decay products in room air. *Health Physics*, *34*(5), 465–473. https://doi.org/10.1097/00004032-197805000-00007

Rajala, M., Kulmala, V., Lehtimaki, M., Janka, K., & Graeffe, G. (2004). The influence of an electrostatic precipitator and a mechanical filter on Rn decay products. *Health Physics*, *50*(4), 447–455. https://doi.org/10.1097/00004032-198604000-00001

Robinson, M. (1919). A modified deutsch efficiency equation for electrostatic precipitation. *Atmospheric Environment, 1*, 193–204. https://doi.org/10.1016/0004-6981(67)90001-7

Royer, G. H. (1954). PatentUS2783384A.

Rudnick, S. N., Hinds, W. C., Maher, E. F., & First, M. W. (1983). Effect of plateout, air motion and dust removal on radon decay product concentration in a simulated residence. *Health Physics*, *45*(2), 463–470. https://doi.org/10.1097/00004032-198308000-00022

Ruttanachot, C., Tirawanichakul, Y., & Tekasakul, P. (2011). Application of electrostatic precipitator in collection of smoke aerosol particles from wood combustion. *Aerosol and Air Quality Research*, *11*(1), 90–98. https://doi.org/10.4209/aaqr.2010.08.0068

Stevanovic, N., Markovic, V. M., & Nikezic, D. (2010). Relationship between deposition and attachment rates in Jacobi room model. *Journal of Environmental Radioactivity*, *101*(5), 349–352. https://doi.org/10.1016/j.jenvrad.2010.02.002

Townsend, J. S. E. (1915). *Electricity in gases*. Clarendon Press.

Tracerlab Gmbh. (n.d.). *Tracerlab Radon daughter monitor BWLM-PLUS-2S*. www.tracerlab.com

United Nations Scientific Committee on the Effects of Atomic Radiation. (2000). Sources and effects of ionizing radiation. In *UNSCEAR 2000 Report*. https://doi.org/10.18356/49c437f9-en

United Nations Scientific Committee on the Effects of Atomic Radiation. (2008). Sources and effects of ionizing radiation. In *UNSCEAR 2008 Report*. https://doi.org/10.2307/3577647

White, H. J. (1962). *Industrial electrostatic precipitation* (First ed.). Addison-Wesley Publishing.

White, H. J. (1974). Resistivity problems in electrostatic precipitation. *Journal of the Air Pollution Control Association*, *24*(4), 313–338. https://doi.org/10.1080/00022470.1974.10469923

World Health Organization. (2010). WHO handbook on indoor Radon: A public health perspective. In *World Health Organization* (Vol. 67).

Yehia, A., Abdel-Salam, M., & Mizuno, A. (2000). On assessment of ozone generation in dc coronas. *Journal of Physics D: Applied Physics*, *33*(7), 831–835. https://doi.org/10.1088/0022-3727/33/7/312

Yuan, L., Luo, B., Wang, J., Wu, J., & Geng, S. (2016). *Research on electrostatic-filtration Radon elimination techniques in underground space*. *IFEESD*, 24–30. https://doi.org/10.2991/ifeesd-16.2016.5